Simulations of aerosol aggregation including long-range interactions

V. Arunachalam,[1,*] R. R. Lucchese,[2] and W. H. Marlow[1]
[1]*Department of Nuclear Engineering, Texas A&M University, College Station, Texas 77843*
[2]*Department of Chemistry, Texas A&M University, College Station, Texas 77843*
(Received 22 July 1998; revised manuscript received 4 March 1999)

Current understanding of solid aerosol particle aggregation is limited to simulation models based on diffusive and ballistic motion of the colliding particles. The role of the long-range van der Waals forces in aggregation phenomena, although important, has never been examined. In an effort to address this issue, a simulation model, based on molecular dynamics techniques, is developed. Using this model to simulate thermal collisions of single spheres with small aggregates of similar spheres, we examine the effects of retardation of the long-range van der Waals forces, particle transport, ambient temperature, and pressure on the collision rates and mass and structure distributions of the aggregated particles. The model calculations were performed at simulated temperatures of 293 and 1500 K and at simulated pressures of 760 and 3040 torr for glassy carbon primary particles in the free molecular regime with diameters of 6 nm, and in the transition regime with diameters of 30 nm. Inclusion of the long-range van der Waals forces resulted in aggregates with relatively open structures and few branches and collision rate constants that were larger than the corresponding hard sphere rate constants, whereas exclusion of the forces resulted in compact structures with more branches and smaller enhancements in the rate constants. The above effects were found to be more pronounced in the free molecular regime than in the transition regime, which is consistent with the observation that the initial conditions and the interparticle forces play a more significant role in particle transport in the free molecular regime than in the transition regime. The effect of retardation of the forces is an increase in the percentage of open aggregates and the collision rate constants over that of the corresponding nonretarded case. An increase in temperature resulted in a collapse of aggregate structure and a decrease in collision rate constants corresponding to the reduced geometrical cross sections. Again, the effects were found to be more pronounced in the free molecular regime than in the transition regime. No significant difference was observed in the structure of the aggregates or in the collision rate constants with a change in pressure, indicating that the pressure effect, if any, is hidden by the much stronger effect of the long-range van der Waals forces. [S1063-651X(99)11508-3]

PACS number(s): 82.70.Rr, 61.43.Hv, 61.46.+w

I. INTRODUCTION

Solid ultrafine aerosol particles with diameters ranging from 1 to 100 nm are produced by a number of natural and artificial processes. Examples include, but are not limited to, combustion, atmospheric photochemical reactions, volcanic eruptions, and gas phase materials synthesis. Experimental observations [1–3] indicate that after their formation many of the initially dispersed spherical particles collide and stick together to build aggregates with irregular and open structures. However, the physical basis (or interaction forces) underlying the evolution of these aggregates and the corresponding collision rate constants have not been examined.

Practical implications of the aggregation process are as varied as they are numerous. For example, in processes involving condensation, the shape of the aggregates is a critical factor in determining the onset of condensation [4,5]. In gas phase materials processing, the formation and growth of aggregates prior to deposition can affect either constructively or destructively the properties and ultimate usefulness of the deposit.

For the simplest case, the collision between two spherical particles, several investigators [6–8] found better agreement between their experimentally observed collision rates and theoretical calculations when they included the attractive long-range van der Waals interaction energy in their coagulation calculations. Inclusion of this interaction energy is particularly important in the case of collisions between free molecular regime aerosol particles [9], which have characteristic dimensions much less than the gas molecular mean free path λ_g, since such collisions are governed by particle-particle interactions and initial conditions. While the calculation of the long-range van der Waals (vdW) energy for spherical particles is straightforward, calculations for aggregated particles comprised of several such spherical particles are complex, and have only recently become available [10]. This interaction energy and its derived force are important elements in a dynamical study the aggregation process.

Several simulation models are available in the literature for aggregate growth. They can be broadly classified as kinetic [11] and dynamic models [3,12]. Kinetic models such as the Eden model [13], the Vold [14] and Sutherland [15] models, and the diffusion-limited aggregation (DLA) model [16] rely on a purely random kinetic mechanism to model aggregate growth. While such models are suitable for some physical processes, they are not suitable for aggregation studies involving ultrafine aerosol particles, because the growth mechanism in the kinetic models depends only on the geometric features of the aggregate, while ignoring the physical forces between the particles and the energy consid-

*Present address: Motorola Inc., 3501 Ed Bluestein Blvd., MD-K10, Austin, TX 78721.

erations. Dynamic models, such as the models based on the Langevin equation of motion, have been used more recently to study aerosol particle aggregation [3,12]. In these models, the interaction between the particle and the gas is treated in a statistical manner. The force on the Brownian particle is assumed to be composed of two parts: a frictional force which is proportional to the Brownian particle velocity, and a randomly fluctuating force. The free molecular condition is incorporated through proper choice of the particle relaxation time β, i.e., $\beta\tau \ll 1$, where τ is the time taken to free stream one particle diameter. Samson, Mulholland, and Gentry [3] applied the Langevin equations to cluster-cluster aggregation, and found that their approach better represented the soot aggregation process than the DLA model of Witten and Sander. However, when the Brownian particle experiences additional interactions, such as the long-range vdW interactions, models based on molecular dynamics simulation techniques are particularly useful.

The primary objective of this paper is to present a physically realistic simulation calculation of the early stages of aerosol aggregation by including the long-range vdW energy in the calculations of the collision rates of single spheres with small aggregates of similar spheres, and to examine the effect of this energy on collision rate constants for the process as well as the effect on the aggregate structures. The work also examines several related issues which have not been addressed adequately in the literature, such as the the effects of retardation of the long-range intermolecular forces [17], particle transport, ambient temperature, and pressure on the collision rate constants, and mass and structure distributions of the aggregates.

This paper is structured as follows: In Sec. II we describe the various features of the simulation model based on molecular dynamics. In Sec. III we outline the case studies performed using the model. In Sec. IV we describe the quantities used to characterize the morphology of the aggregates. In Sec. V we discuss the results of the case studies. Finally, in Sec. VI we present our conclusions.

II. SIMULATION MODEL

The simulation model is based on molecular dynamics methods [18,19]. Given the initial conditions, such as particle positions and velocities, and the interparticle forces (the long-range vdW forces), the equations of motion of the particles are solved. The trajectories are terminated when the particles come into contact, at which time adhesion will be assumed or the trajectories are continued until they can be classified as nonreactive. The rate constants for the aggregation process and structure distributions are obtained by simulating an ensemble of such collision trajectories over thermal distributions of initial conditions.

In the initial stages of aggregation, because of the high monomer concentration, aggregate growth occurs primarily by monomer addition. In the later stages, the monomer concentration becomes depleted, and aggregate-aggregate (or cluster-cluster) collisions become increasingly important in the growth process. Several authors have studied cluster-cluster agglomeration. At this point, it is helpful to differentiate between the use of the terms aggregation and agglomeration. Aggregation refers to the process in which individual particles are added one at a time to a growing cluster. The present model, along with the models of Vold [14] and Witten and Sander [16], fall under this category. Agglomeration, on the other hand, refers to the growth process in which clusters collide and adhere to each other. Examples of agglomeration models include those of Meakin [20], Kolb, Botet, and Jullien [21], and Mountain, Mulholland, and Baum [22].

The objective of our model is to simulate the formation of aggregated particles in the initial stages, because it is these aggregates that serve as ''seed particles'' for subsequent growth by agglomeration. The aggregate's growth is modeled by an iterative process. We begin the process by simulating an ensemble of dimer-monomer trajectories, over thermal distributions of initial conditions. The coordinates of the resulting trimers are stored in a data file. In the subsequent stage, an ensemble of trimer-monomer trajectories are simulated by randomly selecting trimer coordinates from the above mentioned data file. The process was repeated up to an aggregate size of ten particles.

A. Interaction energy

In the initial stages of aggregate growth, because the particle dimensions are much smaller than the mean free path of the gas, transport is primarily collisionless and governed by the interaction energy and initial conditions. Inclusion of the interaction energy is therefore important for physically realistic simulation calculations of aggregate growth. In the case of neutral, nonpolar particles of glassy carbon considered in this study the interaction energy of primary importance is the long-range vdW energy which has its origins in the instantaneous charge fluctuations in atoms and molecules. Glassy carbon was chosen as the prototype material for this study for the following reasons: (1) Carbon is a widely occurring component in many combustion aerosols that have been observed to aggregate to form irregularly shaped particles. (2) Spectroscopic data required for the calculation of the frequency dependent dielectric constant, an input to the interaction energy calculations, are available [23].

Although the role of the long-range vdW energy in spherical ultrafine aerosol particle collisions is well known [9], its effect on the collisions of nanometer spheres with aggregated particles comprised of similarly sized spheres has never been examined. The reason for this is that although the Lifshitz approach [24], which is widely used for the vdW energy calculations, has full generality, and is applicable to any body at any temperature, analytical expressions for the interaction energy can be obtained only for the case of separable coordinates and therefore limited physical geometries. This issue was recently addressed and overcome by Arunachalam, Marlow, and Lu [10]. They calculated the total interaction energy between an aggregated particle and a single spherical particle, first by considering the molecular structure of the particles (discrete picture), and second by considering them to be condensed matter spheres (continuum picture). In the first picture, by comparing the completely coupled, iterated-dipole energies between the constituent molecules [25] with the energy calculated by ignoring the coupling between the molecules of the contacting particles in the aggregate, they showed that the effect of the coupling on the total interaction energy was small. Next, using the second

TABLE I. The parameters (in units of 10^{-13} erg) used in Eq. (1) to fit the retarded van der Waals energy for a pair of glassy carbon spherical particles of diameter 6 and 30 nm, respectively, at 293 K.

Parameters	Values for 6-nm particles	Values for 30-nm particles
a_1	1.9769×10^{-2}	-3.5469×10^{-3}
a_2	-3.4087×10^{-1}	-3.3930×10^{-2}
a_3	-2.6766	-0.1377
b_1	-13.6562	-0.2095
b_2	-15.2962	4.5162×10^{-2}
b_3	-4.0701	-3.0636×10^{-3}
b_4	-0.8228	-1.1343×10^{-4}
b_5	-5.0795×10^{-2}	-1.9891×10^{-6}
b_6	-2.3035×10^{-3}	-1.8516×10^{-8}
b_7	-1.4169×10^{-5}	-5.0549×10^{-11}
b_8	-3.6786×10^{-8}	1.6118×10^{-15}
b_9	7.9035	1.3513
b_{10}	34.6621	2.1049
b_{11}	3.4407×10^{-2}	-4.6393×10^{-5}

(continuum) picture, they computed the total interaction energy as a simple sum of the Lifshitz energies between the individual particles. They found that there was close correspondence between this energy and energies calculated in the discrete picture, thereby indicating that the error made in calculating the total interaction energy as a simple sum over individual Lifshitz energy values is small. For the ultrafine particles considered here, energy calculations based upon the discrete picture would be clearly impractical because of the large number of molecules involved. The Arunachalam-Marlow-Lu method described above provides a simplified, yet effective and computationally feasible method, for calculating the long-range vdW energy between aggregated particles of any shape and size. It also takes into account the effect of retardation on the long-range vdW energy. This effect causes the magnitude of the interaction energy to fall off more rapidly ($1/d^7$, where d is the surface-to-surface separation between the particles) than the corresponding nonretarded energy ($1/d^6$).

At contact separations, the vdW energy becomes singular. The problem of singularity arises because the molecules are assumed to be point particles. Lu, Marlow, and Arunachalam [26] showed that when the finite size of the molecule is taken into account, the singularity problem is removed. Also, as the surface-to-surface separation between the particles increases, and molecular size effects become decreasingly important, the short-range energy converges smoothly to the continuum energy calculated using the Lifshitz approach. Below we present a parametrized representation [10] of the retarded vdW interaction energy used in our simulation calculations. It is valid over all separations (including contact separation)

$$E(d)=\frac{1+a_1d+\cdots+a_{n-1}d^{n-1}}{b_1+b_2d+\cdots+b_{n+7}d^{n+6}}. \tag{1}$$

The parameter values are listed in Table I, and are chosen such that when $d=0$, Eq. (1) gives the correct value for the contact energy, and as $d\to\infty$, $E(d)\to C_{\mathrm{LIF}}d^{-7}$, where C_{LIF} is the Lifshitz constant. The parametrized representation is easily programmed, and is particularly beneficial to simulation calculations, based on molecular dynamics, where considerable time is spent on the evaluation of the interparticle forces.

B. Particle transport

An understanding of particle transport in a gas is central to simulations of aerosol particle collisions by trajectory calculations. To quantify the role of the gas in transport processes involving aerosol particles, the particle Knudsen number [27] is conventionally defined as $\mathrm{Kn}=\lambda_g/r_p$, where λ_g is the gas molecular mean free path and r_p is the particle radius. In these terms, the kinetic condition $\mathrm{Kn}\leqslant0.25$ is termed the collision-dominated or continuum regime, since the gas can be treated as a fluid or continuum. The condition $\mathrm{Kn}\geqslant10$ is termed the free molecular regime, since particle-gas collisions are isolated allowing the particles to follow primarily collisionless trajectories as is the case for individual molecules in a dilute gas. The transition regime $0.25\leqslant\mathrm{Kn}\leqslant10$ falls between the collision-dominated and free molecular regimes.

Modeling the transport of aggregating particles can be a complex undertaking, especially when their sizes are increasing and their shapes are evolving as is the case in a simulation of aggregate growth. In the beginning stages of growth, the colliding particle dimensions could very well be much less than the mean free path of the gas, in which case the transport is primarily collisionless and governed by the interaction potential and initial conditions. However, as the aggregate grows and its greatest dimension becomes comparable to the gas mean free path, the transport enters the transition regime, a region in which particle transport is neither completely free molecular nor completely continuum. In an effort to account for particle transport as the aggregate grows, in a consistent and physically meaningful way, we adopt Fuchs' concept [28] of the jump distance. Our reason for using this pragmatic approach is motivated by good agreement between experimentally determined collision rates for spherical particles [6,7,8] and results derived from Fuchs' semiempirical formulation for the collision rates as generalized to include the long-range intermolecular forces [9]. To our knowledge, this is the first time that Fuchs' concept has been incorporated into simulation calculations of aerosol aggregation. In this model, the jump distance δ_{AB} for two particles of radii r_A and r_B diffusing toward each other represents the mean surface-to-surface distance between the colliding particles for which the motion can be considered as free molecular. Fuchs' model was to utilize the classical diffusion theory only for a center-to-center separations between the particles, $d_0>r_A+r_B+\delta_{AB}$. Then, in this model for $d_0<r_A+r_B+\delta_{AB}$, the particles move according to the kinetic theory of gases as if in vacuum. By equating the particle fluxes from the two transport domains at $d_0=r_A+r_B+\delta_{AB}$ he obtained an expression for the jump distance as

$$\delta_{AB}=(\delta_A^2+\delta_B^2)^{1/2}, \tag{2}$$

where δ_{AB} is the thermal average of the individual particle jump distances δ_A and δ_B. δ_A is given by

$$\delta_A = \frac{1}{6 r_A \lambda_A}[(2r_A+\lambda_A)^3-(4r_A^2+\lambda_A^2)^{3/2}]-2r_A, \quad (3)$$

where λ_A denotes the particle mean free path.

In the case of two spherical particles the free molecular region, according to Fuchs' approach, is defined by a spherical ''envelope'' that extends for a distance δ_{AB} around the surface of the particles. However, the definition of such an ''envelope'' for a system comprised of an aggregate and a monomer is not straightforward because of the irregular shape of the aggregate. Assuming for the moment that δ_{AB} can be calculated for such a system, by an extension of the Fuchs' approach, we define the ''envelope'' as the irregular surface that follows the contour of the aggregate at a distance δ_{AB} from it. In our simulation model for collisions between aggregates and monomers, the motion of the colliding particles is simulated only in the free molecular region bounded by the so-called ''envelope.'' The procedure involves separating the aggregate and monomer, initially, by a center-to-center distance d_0 given by

$$d_0 = r_A^{\max} + r_B + \delta_{AB}, \quad (4)$$

where $r_A^{\max}$ is the maximum possible aggregate radius, for a given number of constituent particles, i.e., the radius of the linear aggregate, r_B is the monomer radius, and δ_{AB} is the thermally averaged jump distance for the aggregate-monomer system. The colliding particles are then propagated along a straight line trajectory (in the absence of the interaction potential) until the surface-to-surface separation between the monomer and any particle in the aggregate is less than or equal to δ_{AB}, at which point the interaction potential is turned on. Subsequently, the motion of the particles is propagated by solving their equations of motion, with the long-range vdW force, until they collide or until the trajectory can be classified as a nonreactive one. The diffusive motion of the particles prior to the point where the potential is turned on, although not explicitly modeled, is implicitly accounted for by randomly rotating the aggregate prior to propagation. This ensures random relative orientations of the aggregate and monomer as is the case in diffusive motion, albeit without the minor effects of long-range forces at these relatively large separations.

To define the boundary for our calculations, we require a mean free path λ_A for the aggregated particle. This is evaluated by assuming that it is equal to the mean free path for a spherical particle that has the same drag force as the aggregate. Obviously this assumption precludes anisotropic drag. Since the drag force is directly related to the mean persistence distance, we thereby have the required relationship.

Assuming that the drag force on the aggregate [29] increases as its projected surface area and its radius of gyration, it follows that the ''equivalent'' sphere is one that has the same radius of gyration as the aggregate. The hard sphere radius of this ''equivalent'' sphere is given by

TABLE II. Variation of jump distance δ with temperature and aggregate size for primary particles of diameter (a) 6 nm and (b) 30 nm. δ_A denotes the jump distance for a monomer or an aggregate. δ_{AB} denotes the thermally averaged jump distance for a monomer-aggregate system. r_B is the monomer radius. Note that all aggregates are linear.

N	δ_A/r_B at 293 K	δ_{AB}/r_B at 293 K	δ_A/r_B at 1500 K	δ_{AB}/r_B at 1500 K
		(a) 6 nm		
1	7.7	10.9	30.8	43.6
2	4.0	8.7	17.0	35.3
3	1.5	7.8	7.3	31.7
7	0.3	7.7	1.3	30.8
10	0.2	7.7	0.7	30.8
		(b) 30 nm		
1	0.53	0.75	2.43	3.44
2	0.27	0.60	1.17	2.70
3	0.13	0.53	0.47	2.51
7	0.03	0.53	0.10	2.43
10	0.03	0.53	0.07	2.43

$$r_{\rm hs} = (\tfrac{5}{2})^{1/2} r_g, \quad (5)$$

where the radius of gyration of the aggregate r_g is defined by

$$r_g = \left(\frac{\sum_i m_i r_i^2}{\sum_i m_i} \right)^{1/2}, \quad (6)$$

where m_i denotes the mass of the constituent particles, and r_i their distance from the aggregate center of mass. The factor $(\frac{5}{2})^{1/2}$ in Eq. (5) arises from the relationship between the hard sphere radius and radius of gyration of a sphere. Substituting Eq. (6) into Eq. (5) now gives the radius r_A to be used in Eq. (3) for the aggregate jump distance calculation. Tables II(a) and II(b) list the jump distances as a function of temperature and aggregate size for primary particles of diameter 6 and 30 nm, respectively. For simplicity, only the results for linear aggregates are presented. It can be seen from the tables that, in general, the jump distance for an aggregate-monomer system, δ_{AB}, is bracketed by the monomer jump distance in the lower limit and the jump distance of a monomer-monomer system in the upper limit. The lower limit is realized for the large aggregates ($N=7,10$) for which $\delta_A \to 0$. Also, for a fixed primary particle size, as the temperature increases, the jump distance increases due to a decrease in the gas density and a corresponding increase in the mean free path of the particles. For a constant temperature, the jump distance decreases with increasing primary particle size. This is because the particle size now becomes comparable to its mean free path and the gas-particle collisions become more frequent; consequently the distance over which the particle motion can be regarded as collisionless, i.e., the jump distance is reduced.

C. Thermal collision rates

Consider the reaction of particles A and B, where A and B denote the aggregate and monomer, respectively. If Λ is a reaction channel, then the reaction rate for this channel is given by

$$\Re(A,B)=R_{\Lambda}(A,B)[A][B], \tag{7}$$

where $[A]$ and $[B]$ are the concentrations of particles A and B, and $R_{\Lambda}(A,B)$ is the rate constant for the reaction channel Λ. In this study, the reaction channel of interest is sticking. It is assumed that the particles adhere upon contact because of the availability of a large number of vibrational modes of the system to dissipate, or thermalize, the collisional energy [30,31]. The rate constant for the sticking reaction is given by

$$R_s(A,B)=\left(\frac{8kT}{\pi\mu}\right)^{1/2}\sigma_s(A,B), \tag{8}$$

where k is the Boltzmann constant, and μ the reduced mass. The first term is the average thermal velocity, and the second term is the cross section integral for the sticking reaction given by

$$\sigma_s(A,B)=\int 2\pi b\,\frac{E_{\rm coll}e^{-[E_{\rm coll}/(kT_{\rm coll})]}}{(kT_{\rm coll})^2}\,\frac{e^{-[E_{p_A}/(kT_A)]}}{Z_{p_A}} \times P_{\Lambda}(b,E_{\rm coll},E_{p_A},\varphi_A,\psi_A,\theta_A)\,\frac{d\varphi_A}{2\pi}\,\frac{d\psi_A}{2\pi} \times\left(\frac{\sin\theta_A d\theta_A}{2}\right)dp_A dE_{\rm coll}db, \tag{9}$$

where $T_{\rm coll}$ is the mean collisional temperature, b is the initial impact parameter, $E_{\rm coll}$ is the initial collision energy, and E_{p_A} and p_A are the rotational energy and $3N_A$ momenta of the rigid aggregate, respectively. Z_{p_A} is the rotational partition function of the aggregate, and φ_A, ψ_A, and θ_A are the angles that define the relative orientation of cluster A with respect to the axis passing through its center of mass along which the collision is initiated. $P_s(b,E_{\rm coll},\ldots)$ is the normalized probability density function for the sticking reaction. The limits of integration for the integral over b and $E_{\rm coll}$ are $(0,\infty)$. For the momenta of the rigid aggregate the limits of integration are $(-\infty,+\infty)$. For the angles φ_A and ψ_A, the limits are $(0,2\pi)$ and for θ_A the limits are $(0,\pi)$. Due to the complexity of the rate constant integral [Eq. (9)], an analytical solution cannot be obtained except for very simple cases. However, the integral can be evaluated in the classical trajectory method [32,33,34] using standard Monte Carlo integration techniques [32].

In this method, an ensemble of collision trajectories are simulated over thermal distributions of initial conditions, up to the points of contact at which times adhesion will be assumed or until the trajectories can be classified as nonreactive. The rate constant for a collision reaction that results in sticking is then calculated by

$$R_s(A,B)=\left(\frac{8kT}{\pi\mu}\right)^{1/2}\lim_{b_{\max}\to\infty}\pi b_{\max}^2\lim_{N\to\infty}\frac{N_s}{N}, \tag{10}$$

where N is the total number of trajectories simulated and N_s is the number of trajectories that result in a sticking reaction. The relative statistical error introduced by replacing the rate constant given by Eq. (9) with the one given by Eq. (10) can be readily estimated [29] for large N to be $[(N-N_s)/N_sN]^{1/2}$. We can easily see that for $N_s \ll N$, the relative statistical error goes as $N_s^{-1/2}$. The square root dependence means a moderate accuracy can be achieved with a relatively small number of trajectories, while greater accuracy would require a significantly larger number of trajectories.

The initial impact parameter for each collision is chosen from a normalized b^2 distribution,

$$f(b)db=\begin{cases}\dfrac{2\pi b db}{\pi b_{\max}^2}, & 0<b<b_{\max}\\ 0 & \text{otherwise,}\end{cases} \tag{11}$$

where $b_{\max}$ is the maximum impact parameter, which, according to classical collision theory, is infinite. For simulation purposes, however, setting an infinite limit for the impact parameter is impractical. Therefore, it is necessary to devise a method whereby an optimal value for $b_{\max}$ can be selected. One such method is stratified sampling [35] which has been used by several authors [31,33,35] in the context of molecular dynamics simulations. The selection process for the optimal $b_{\max}$ is an iterative one, as it is based on the convergence of the collision rate constant computed using Eq. (10). For a fixed $b_{\max}$, the range of b values is divided into bins:

$$\begin{array}{ll}1\text{st subset} & 0\leqslant b<\beta\\ \vdots & \vdots\\ i\text{th subset} & (i-1)\beta\leqslant b<i\beta\\ \vdots & \vdots\\ I\text{th subset} & (I-1)\beta\leqslant b<I\beta.\end{array}$$

The number of trajectories selected from the ith bin is proportional to the incremental increase in the total collisional area associated with the bin:

$$\lim_{N\to\infty}\frac{N_i}{N}=\left(\frac{\pi(2i-1)\beta^2}{\pi(I\beta)^2}\right). \tag{12}$$

The advantages of the stratified sampling method are (1) It avoids an *ad hoc* definition of $b_{\max}$ and, (2) it leads to very efficient trajectory sampling, thus saving computational time. When using stratified sampling, Eq. (10) for the rate constant must be modified as

$$R_s(A,B)=\left(\frac{8kT}{\pi\mu}\right)^{1/2}\pi b_{\max}^2\sum_{i=1}^{i_{\max}}\frac{N_{si}}{N_i}\left[\frac{b_i^2-b_{i-1}^2}{b_{\max}^2}\right], \tag{13}$$

where b_i and b_{i-1} are the upper and lower limits of the ith bin, N_i is the number of trajectories sampled in the ith bin, and N_{si} is the number of trajectories that result in a collision or sticking event in that bin. The estimated error in the rate constant calculated using Eq. (13) is

$$\Delta R_s(A,B)=\left(\frac{8kT}{\pi\mu}\right)^{1/2}\pi b_{\max}^2\left\{\sum_{i=1}^{i_{\max}}\left[\frac{(N_i-N_{si})N_{si}}{N_i^3}\right]\times\left[\frac{b_i^2-b_{i-1}^2}{b_{\max}^2}\right]^2\right\}^{1/2}. \quad (14)$$

In our simulations of cluster-monomer collisions, the initial estimate for $b_{\max}$ is of the order of several monomer diameters, at which the long-range vdW forces between the colliding particles are negligible. Stratified sampling is then performed, and the bins in which no sticking (collisions) occurs are eliminated resulting in a new value for $b_{\max}$. The process is repeated until the collision rates obtained from two successive iterations converge. For all the final converged cases, the estimated error in the rate constant given by Eq. (14) was found to be at least two orders of magnitude less than the value of the rate constant. The details relating to the setup and simulation of the individual collision trajectories are outlined below.

D. Trajectory initialization

The initial setup for the aggregate, prior to propagation, involves two steps [36] which ensure that the aggregate has rotational motion consistent with the ambient temperature and that its rigidity is maintained despite the rotation imparted to it. The two step procedure is as follows.

(1) Sample atomic Cartesian velocities $\{v_i'\}_{i=1,N}$ as independent Gaussian variables such that

$$\langle v_{i\alpha}'\rangle=0, \quad (15)$$

$$\langle v_{i\alpha}'^2\rangle=kT, \quad (16)$$

where $\alpha=x,y,z$ and the average is taken over an ensemble of aggregates, each comprised of N spherical particles.

(2) Subtract from the velocities their components ''normal'' to the constraint surfaces in the $3N$ Cartesian hyperspace in order to allow the constraints' time derivatives to vanish. This is written

$$\vec{v}_i=\vec{v}_i'-\sum_{k=1}^{l}\lambda_k\frac{\partial\varepsilon_k}{\partial\vec{r}_i} \quad i=1,\ldots,N, \quad (17)$$

where l denotes the number of holonomic constraints, ε_k, of the system. Details pertaining to these constraints will be discussed in Sec. II E. The $\{\lambda_k\}$ parameters are fixed by requiring that

$$\frac{d\varepsilon_k}{dt}=\sum_{j=1}^{N}\frac{\partial\varepsilon_k}{\partial\vec{r}_j}\vec{v}_j=0, \quad k=1,\ldots,l. \quad (18)$$

Combining Eqs. (17) and (18), and solving for $\{\lambda\}$, one obtains

$$\lambda_k=\sum_{k'=1}^{l}(Z^{-1})_{kk'}\sum_{i=1}^{N}\frac{\partial\varepsilon_{k'}}{\partial\vec{r}_i}\vec{v}_i', \quad (19)$$

where Z is an $l\times l$ matrix defined by

$$Z_{ij}=\sum_{k=1}^{N}\frac{1}{m_k}\frac{\partial\varepsilon_i}{\partial\vec{r}_k}\frac{\partial\varepsilon_j}{\partial\vec{r}_k}, \quad i,j=1,\ldots,l, \quad (20)$$

$$\varepsilon_k\equiv(\vec{r}_i-\vec{r}_j)^2-\gamma_{ij}^2=0, \quad i>j=1,\ldots,n_b, \quad k=1,\ldots,l, \quad (21)$$

where γ_{ij} denotes the bond length and n_b is the number of bonds. As a result of this initialization procedure, the aggregate rotates as a rigid body but has no translational motion. To avoid any orientational correlations, the aggregate is rotated randomly through Euler angles about its internal axes prior to the initialization procedure described above.

The colliding bodies, the rigidly rotating aggregate, and the monomer are initially separated, along the z axis, by a distance d_0 which is determined using Fuchs' approach described in Sec. II B. The initial impact parameter b is selected randomly using the stratified sampling technique described in Sec. II C. The bodies are then separated by b along the y axis. At this initial separation, which is typically several monomer diameters, the interparticle long-range vdW energy is negligible compared to the thermal energy. The relative center of mass collision energy, E_{coll}, which determines the collision velocity, is selected randomly from the normalized Boltzmann distribution corresponding to the ambient temperature T,

$$f(E_{\text{coll}})dE_{\text{coll}}=(kT)^{-2}E_{\text{coll}}\exp\left(\frac{-E_{\text{coll}}}{kT}\right)dE_{\text{coll}}. \quad (22)$$

This assures an average center of mass collision energy of $2kT$.

E. Trajectory simulation and the method of constraints

The propagation of the equation of motion of the monomer is straightforward, and is performed using the Verlet algorithm [37]. However, the propagation of the equations for the particles comprising the rigid aggregate subject to external forces, which in this case is the long-range vdW forces, is not straightforward. There are two different ways to express the equations of motion for this rigid system.

(1) One can use equations of motion in generalized coordinates involving nonconstrained degrees of freedom. For rigid bodies, this leads to Newton-Euler equations, in principle very simple. In practice, numerical difficulties are encountered with Euler angle variables which require the introduction of special integration schemes.

(2) Alternatively, one can use equations of motion in the Cartesian coordinates of all particles comprising the aggregate, modified so as to satisfy the system constraints. The Cartesian equations of motion now are governed by a total force which is given as the sum of the forces derived from the potential energy and the force arising from the constraints. The forces of constraint depend upon a set a Lagrange multipliers which are evaluated from the constraint relationships by auxiliary calculations. This method can be applied easily to even complex aggregates, and can be done in a way that is computationally very effective. Its implementation, the so-called method of constraints, was developed for rigid polyatomic systems by Cicotti and his coworkers in a series a publications that can be found in Ref. [37]. In this simulation model we use the method of constraints because, in addition to the advantages mentioned

above, it is a Cartesian coordinate approach, and therefore, has the virtue of simplicity.

The trajectory simulation is terminated when either a sticking event (physical contact) occurs between the aggregate and monomer or when the trajectory can be classified as a nonreactive one, in which case the following conditions must be satisfied simultaneously: (1) the monomer kinetic energy exceeds the monomer-aggregate interaction potential energy, and (2) the monomer begins to move away from the center of mass of the aggregate.

III. CASE STUDIES

Using the approach outlined in Sec. II, collisions were first simulated between pairs of spherical particles of varying diameter (6–30 nm). In all cases, good agreement was obtained between the collision rates from simulations and those from analytical calculations based on the generalized Fuchs rate for spheres [9] [for example, $(3.2355\pm0.110)\times10^{-9}\,\mathrm{cm}^3/\mathrm{s}$ vs $3.0399\times10^{-9}\,\mathrm{cm}^3/\mathrm{s}$ for 6-nm particles for simulation and analytical, respectively]. Next, aggregate structure and rate constants for the collision reactions between aggregates of different sizes and monomers were examined for a variety of the simulation conditions. Aggregate growth was simulated with and without the interaction potential to study its effect on the resultant aggregate structure and aggregate-monomer collision rate constants. The effect of retardation of the long-range vdW energy, which causes the interaction energy to fall off more rapidly ($1/r^7$ instead of $1/r^6$), was examined by growing the aggregates with the retarded potential and comparing the results to the simulations performed with the nonretarded potential. Temperature effects were examined by varying the temperature of the simulations, while keeping the particle size and other ambient conditions constant. The temperatures chosen for this study were 293 and 1500 K, since they are representative of, and cover a wide range of, aggregation phenomena, ranging from soot particle aggregation in automobile exhaust pipes to flame synthesis of materials. The primary particle size d_p was varied from 6-nm ($\mathrm{Kn}=22.5$) to 30-nm diameter ($\mathrm{Kn}=4.5$) for each temperature, to examine the free molecular ($\mathrm{Kn}\geqslant10$) and transition regime ($0.25\leqslant\mathrm{Kn}\leqslant10$) effects. The simulations were performed at two different ambient pressures, 760 and 3040 torr, for a constant temperature of 293 K and primary particles of diameter 6 nm. The purpose of this study was to examine the effects of ambient pressure. The results of the above-mentioned case studies are presented in Sec. V.

IV. STRUCTURE DESCRIPTIVES

The structure of aggregates is critical to many phenomena in a variety of fields. For example, various combustion processes release irregularly shaped aggregates into the environment. The condensational growth on these aggregates can be very different from that on equivalent spherical particles, because the equilibrium vapor pressure is dependent on the curvature of the particle surface. It is depressed for negatively curved surfaces, leading to condensation at much lower humidities than over a positively curved surface. Structure descriptives, which give details of the aggregate structure such as its mass distribution and the number of branches, as opposed to those that give information about its gross features, could be extremely beneficial to a quantitative understanding of the relationship between aggregate structure and rates of physical processes.

The literature contains a variety of structure descriptives ranging from the simple, such as the radius of gyration, to the complex, such as the fractal dimension [38]. The structure descriptives used in this study are discussed below. The structures of smallest aggregates grown, the trimers, were analyzed using the angle subtended by the three component particles. The angle, though a very simple measure, gives a clear indication of the degree of openness of the aggregate. The most open structure corresponds to 180°, and the most compact structure to 60°. For larger aggregates ($N=4-10$) the following were the structure descriptives used: (1) radius of gyration, (2) number of branches, and (3) principal moments of inertia.

The radius of gyration (r_g) is a quantitative measure of the mass distribution in the aggregate. The larger the r_g of an aggregate, the more open its structure. However, it is possible that aggregates having equal radii of gyration have very different arrangements of constituent particles. Thus, although r_g is a good measure for aggregate openness, it is not a good indicator of the details of the aggregate structure.

The number of branches in an aggregate, on the other hand, gives detailed information about the connections between the constituent particles. Let us consider an aggregate comprised of N spherical particles. The number of branches is given by the number of particles having a connectivity of 3. The connectivity of a particle is determined by the number of particles adjacent to it.

The gross features of the aggregate, such as its overall shape, were examined by calculating the principal moments of inertia I_{xx}, I_{yy}, I_{zz} ($I_{xx}<I_{yy}<I_{zz}$), and I, their sum, and by examining the relationship between the ratios I_{xx}/I, I_{yy}/I, and I_{zz}/I. The spherical shape corresponds to $I_{xx}/I=I_{yy}/I=I_{zz}/I$, the prolate symmetric top to $I_{xx}/I<I_{yy}/I=I_{zz}/I$, and the oblate symmetric top to $I_{yy}/I=I_{xx}/I<I_{zz}/I$.

V. RESULTS AND DISCUSSION

A. Interaction potential effects

Figure 1 shows the structure distribution function for the smallest aggregates, trimers, grown at 293 K under free molecular conditions. In general, the distribution function is the ratio of the number of aggregates in a bin to the total number of aggregates, and is expressed as a percentage. The distribution function for the trimer case is normalized by the solid angle. It can be seen that when the simulation is performed with the interaction potential on, the trimer structure distribution per unit solid angle is anisotropic, with a large percentage of open timers (100°–180°) and a small percentage of more compact ones (60°–100°). However, without the potential, the trimer distribution is, as expected, isotropic. The effect of the potential on the ''openness'' of the structure is seen for all the aggregate sizes ($N=3-10$) considered here for the aggregates grown under free molecular conditions.

The structures of the aggregates grown under transition regime conditions is somewhat different than those grown

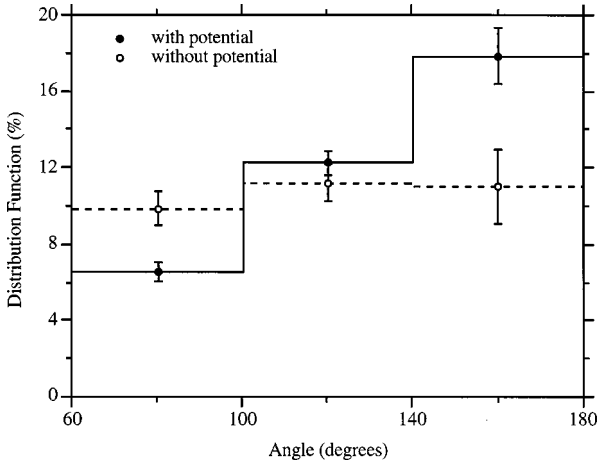

FIG. 1. Normalized trimer structure distribution function vs angle for $d_p = 6$ nm and $T = 293$ K.

under free molecular conditions. For trimers grown at 293 K under transition regime conditions, Fig. 2 shows that the distribution function without potential is fairly isotropic, as is the case for the free molecular regime particles. However, the distribution function with potential is different from the free molecular case. It appears to be less anisotropic in the two outer bins, mainly due to the suppression of the distribution function in the outermost bin. Consequently, the difference between the distribution functions with and without potential is smaller than that in the free molecular case. This effect is also evident for the larger aggregates, and suggests that in the transition regime the interaction potential does not have as strong an influence on particle motion as in the free molecular regime.

Figures 3(a) and 3(b) illustrate the effect of the interaction potential on aggregate morphology through the distribution function for the number of branches for $N = 10$ aggregates. Upon examination of the figures we can see that, at 293 K, for both free molecular and transition regime transport, the aggregate distributions with potential are, on the average, narrower and are peaked when the number of branches is two. A smaller fraction have three and four branches. The fraction of compact aggregates with more complex morphologies (number of branches > 4) is very small. From these observations we can conclude that, as the aggregate grows by monomer addition, the incoming monomer tends to stick to its extremities because of the attractive force between the particles. Without the potential, the aggregate distributions appear to be broader, with more branched aggregates, indicating that the monomer is more likely to travel to the interior of the aggregate before it sticks.

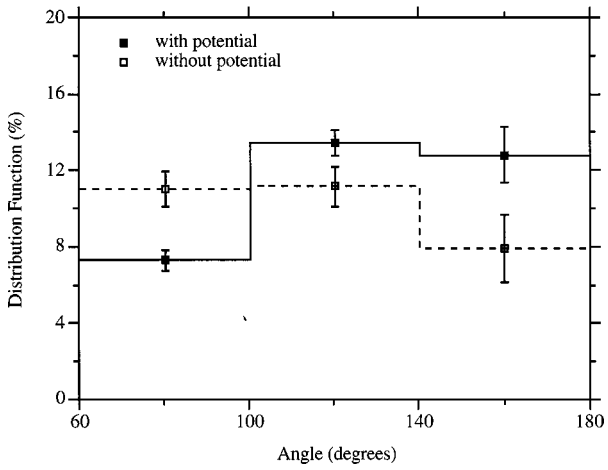

FIG. 2. Normalized trimer structure distribution function vs angle for $d_p = 30$ nm and $T = 293$ K.

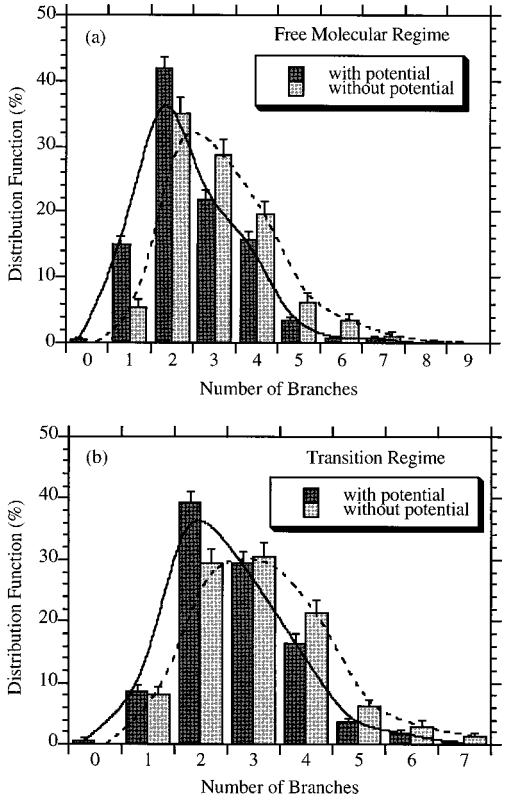

FIG. 3. Connectivity deviation for (a) $N = 10$, $d_p = 6$ nm, and (b) $N = 10$, $d_p = 30$ nm at 293 K.

Yet another way of examining the interaction potential effects on aggregate shape is through its principal moments of inertia I_{xx}, I_{yy}, and I_{zz} ($I_{xx} < I_{yy} < I_{zz}$). For the data given in Fig. 4, aggregate shapes can be bracketed between the prolate symmetric top, corresponding to $I_{xx}/I < I_{yy}/I = I_{zz}/I$ (point A), the spherical shape, corresponding to $I_{xx}/I = I_{yy}/I = I_{zz}/I = 1/3$ (point C), and the oblate symmetric top, corresponding to $I_{yy}/I = I_{xx}/I < I_{zz}/I$ (point B). Figures 4(a) and 4(b) are scatter plots of I_{yy}/I vs I_{zz}/I, for a fixed number of aggregates of size $N = 5$, grown at 293 K, with and without the potential, respectively. Comparison of the data point distribution within the limiting triangle shows a much broader distribution for the aggregates grown without the potential. The average value of I_{xx}/I, which is a measure of the departure from the prolate symmetric top is correspondingly higher. The data on radius of gyration, angle, and number of branches also support this observation.

The effect of the interaction potential on aggregate-monomer collision rate constants is measured by calculating the collision rate constant enhancement factor Ψ_p. Ψ_p is defined as the ratio of the rate constant in the presence of the interaction potential (R_p) to that in the absence of the interaction potential (R_0). Table III(a) shows the results of

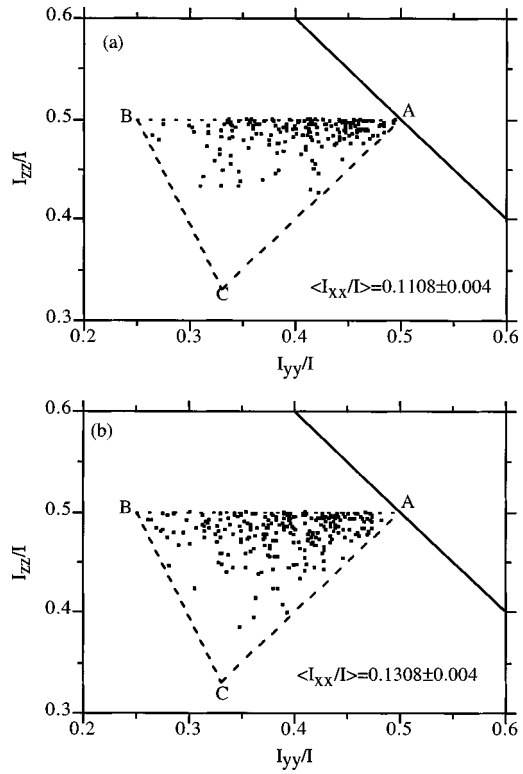

FIG. 4. Scatter plot of I_{yy}/I vs I_{zz}/I for aggregates grown (a) with the potential on, and (b) without the potential at $T=293$ K. $N=5$ and $d_p=6$ nm.

such a calculation for free molecular regime primary particles at 293 K. The enhancement in rate constant that arises purely from geometric considerations is measured by Ψ_0, the ratio of the rate constant for aggregate-monomer collisions without the interaction potential (R_0) to that for collisions between a spherical particle having the same volume as the aggregate and a monomer (R_{hs}). On an average, for aggregates of size $N=2-9$, the aggregate-monomer rate constant is enhanced by a factor of 2.27 ± 0.1 over the corresponding geometric rate constant (or rate constant without the potential). The average value of Ψ_0 for aggregates of size $N=2-9$ is 1.39 ± 0.1. Comparison of the average values of Ψ_p and Ψ_0 shows that the rate constant enhancement due to the pure interaction potential effect is greater than that due to the pure geometric effect by a factor of about 1.6. The aggregate-monomer rate constants and enhancement factors for transition regime primary particles at 293 K are listed in Table III(b). The average value of Ψ_p (1.86 ± 0.1) is lower than that for the free molecular case because of the weaker effect of the interaction potential on particle transport in the transition regime. Ψ_0, however, which is a measure of the enhancement in the rate constant due to the pure geometric effect, should be independent of the transport regime. The constant value of Ψ_0 for both free molecular regime particles [Table III(a)] and transition regime particles [Table III(b)] is consistent with that expectation.

B. Retardation effects

The effect of retardation of the long-range vdW energy increases with particle size, and must be included in a physically realistic description of the aggregation process [39].

TABLE III. Rate constants and rate constant enhancement factors for aggregate-monomer collisions at 293 K for primary particles of diameter (a) 6 nm and (b) 30 nm. N denotes the number of particles in the aggregate. Subscripts indicate the following: p, with potential; 0, without potential; hs, hard sphere.

	Rate constants (10^{-9} cm^3/s)				
N	R_p	R_0	R_{hs}	Ψ_p R_c/R_0	Ψ_0 R_0/R_{hs}
			(a) 6 nm		
2	3.82±0.1	1.61±0.1	1.39	2.37±0.2	1.16±0.1
3	4.69±0.1	1.97±0.1	1.53	2.38±0.1	1.29±0.1
4	5.05±0.1	2.35±0.1	1.67	2.15±0.1	1.41±0.1
5	5.58±0.1	2.39±0.1	1.79	2.33±0.1	1.34±0.1
6	6.12±0.1	2.69±0.1	1.91	2.28±0.1	1.41±0.1
7	6.60±0.1	2.87±0.1	2.02	2.30±0.1	1.42±0.1
8	7.23±0.1	3.31±0.1	2.12	2.18±0.1	1.56±0.1
9	7.57±0.1	3.45±0.1	2.23	2.19±0.1	1.55±0.1
				2.27±0.1[a]	1.39±0.1[a]
			(b) 30 nm		
2	7.48±0.2	3.34±0.1	3.11	2.24±0.1	1.07±0.1
3	8.14±0.2	4.11±0.2	3.43	1.98±0.1	1.20±0.2
4	8.88±0.2	5.10±0.2	3.72	1.74±0.1	1.37±0.2
5	10.10±0.2	5.67±0.2	4.00	1.78±0.1	1.42±0.2
6	11.33±0.2	6.64±0.2	4.27	1.71±0.1	1.56±0.2
7	12.21±0.3	6.49±0.2	4.51	1.88±0.1	1.44±0.2
8	12.73±0.3	6.99±0.2	4.75	1.82±0.1	1.47±0.2
9	13.64±0.3	7.83±0.2	4.98	1.74±0.1	1.57±0.2
				1.86±0.1[a]	1.39±0.2[a]

[a]Average rate constant.

We examined the retardation effect for 30-nm-diameter particles first by performing the simulations with the nonretarded interaction potential from the previous section, and then by comparing the results with those performed with the retarded interaction potential. The nonretarded potential, being the stronger of the two potentials, should result in a higher percentage of more open aggregates, an outcome of the interaction potential's ability to cause large-impact parameter trajectories to stick. In other words, the stronger the interaction potential, the greater the fraction of large-impact parameter trajectories that will result in sticking, and the greater the fraction of more open aggregates. This result is supported, for the simplest case (trimers), by the results presented in Fig. 5. Based on the above arguments, the nonretarded rate constant should also be higher than the retarded rate constant. The results of the dimer-monomer simulations verify this by showing that the nonretarded rate constant is $(7.83\pm0.2)\times10^{-9}$ cm^3/s, while the retarded rate constant is $(7.48\pm0.2)\times10^{-9}$ cm^3/s.

C. Temperature effects

In order to examine the effect of temperature on aggregate structure and aggregate-monomer collision rates in the free molecular and transition regimes, simulations were carried out at both 293 and 1500 K for primary particles of diameter 6 and 30 nm. Before proceeding to a discussion of the results, it is helpful to compare the magnitudes and distance

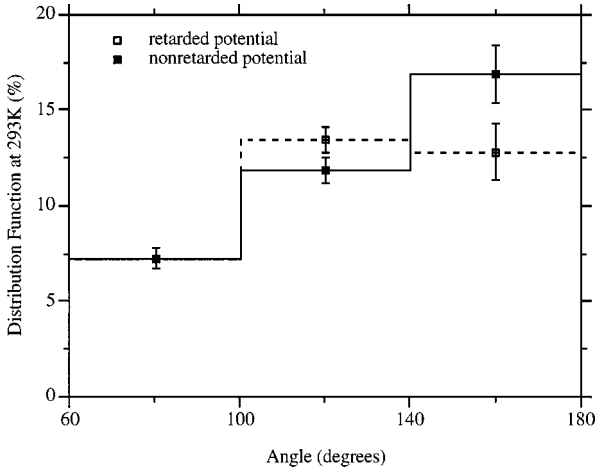

FIG. 5. The retardation effect for $d_p = 30$ nm and $T = 293$ K.

dependences of the interaction potential energy [36]. At 293 K, for both the 6- and 30-nm particles, the interaction energy at contact has finite values of $125kT$ and $700kT$, respectively, and becomes comparable to kT at surface-to-surface separations of $0.56r_p$ and $0.48r_p$, respectively, where r_p denotes the radius of the particle. The interaction potential well is, therefore, much steeper for the 30-nm particle than for the 6-nm particle. At 1500 K, although the magnitude of the interaction energy value does not change appreciably from that at 293 K, the distance at which it becomes equal to kT decreases. Thus, as the temperature increases, the range of the interaction potential, that is, the distance over which it is greater than the thermal energy, decreases.

For the free molecular regime particles (6 nm), comparison of the trimer structures at 293 and 1500 K shows that as the temperature increases: (1) The trimer structure distribution functions, with and without the potential, are similar (Fig. 6), whereas they differ significantly from each other at 293 K (Fig. 1). (2) The percentage of more open trimers (140°–180°) with potential drops significantly (Fig. 7), as a result of which the structure distribution function at 1500 K becomes more isotropic than that at 293 K. This suppression of open structures is also evident for the larger aggregates. The reason for (1) and (2) can be explained as follows. As

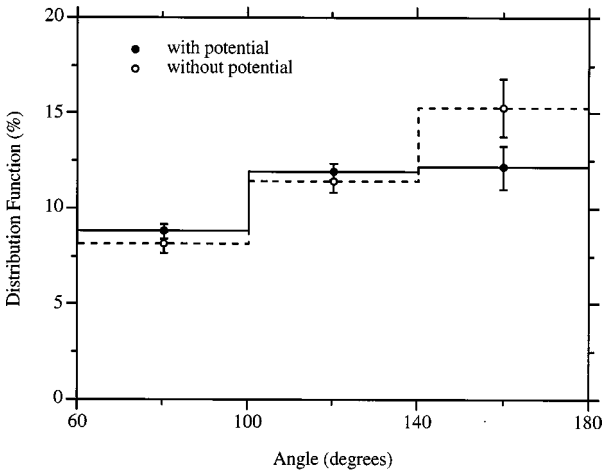

FIG. 6. Normalized trimer structure distribution function vs angle for $d_p = 6$ nm and $T = 1500$ K.

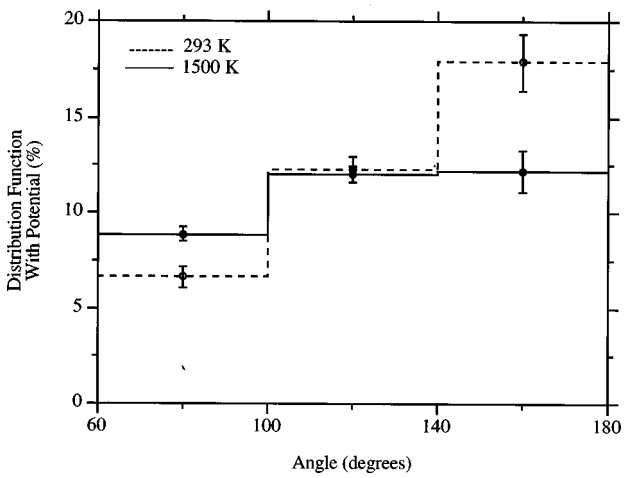

FIG. 7. Comparison of normalized trimer structure distribution functions at 293 and 1500 K for $d_p = 6$ nm.

the temperature increases, the kinetic energies of the colliding particles increase and dominate over the interaction potential energy. This results in linear trajectories which are characteristic of simulations without potential and a convergence of the distribution functions with and without potential (result 1). The almost linear trajectories at 1500 K will result in sticking only if they are within close range of the geometric extent of the aggregate. The chances of a monomer sticking to the aggregate extremities are small. Hence, the resulting aggregates, in this case trimers, are less likely to have more open structures (result 2).

In the transition regime, there is no significant difference in the trimer distribution functions, with potential, at 293 and 1500 K (Fig. 8). The above is true for larger aggregates as well. Although one might expect differences to arise because the jump distance increases with temperature [Table II(b)], this is not evident because (1) the retardation effect decreases the strength of the interaction energy, and (2) the ''range'' of the interaction energy decreases with temperature. Moreover, for the transition regime particles, the collisions are kinetically dominated as opposed to the free molecular regime particles where the collisions are influenced to a greater ex-

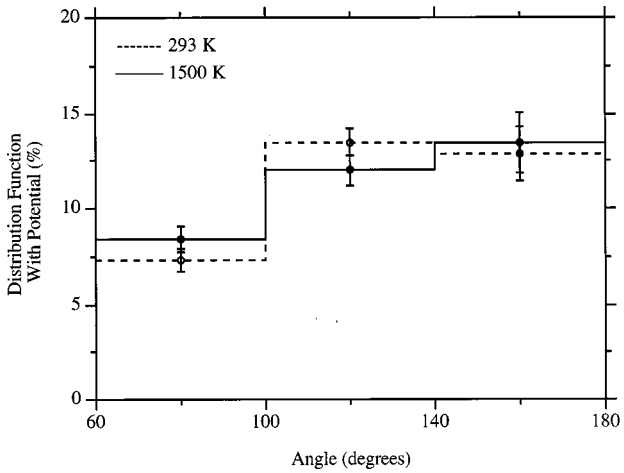

FIG. 8. Comparison of normalized trimer structure distribution functions at 293 and 1500 K for $d_p = 30$ nm.

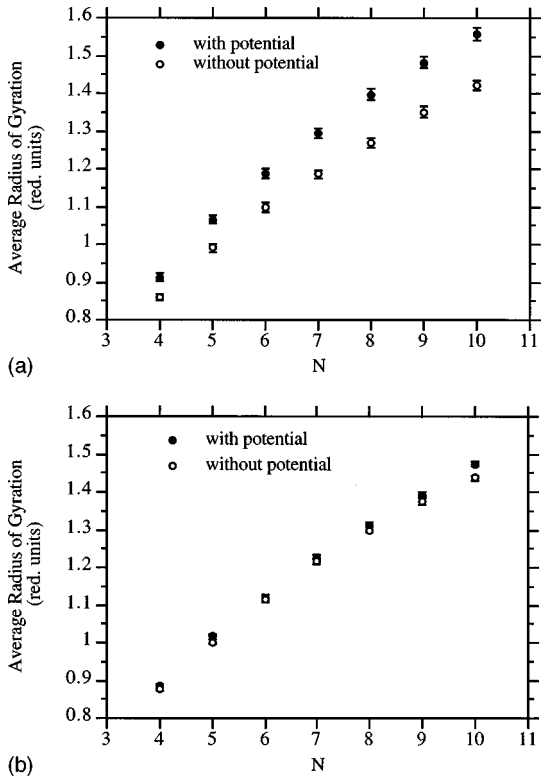

FIG. 9. Interaction potential effect over a range of aggregate sizes for $d_p = 6$ nm at (a) $T = 293$ and (b) 1500 K. The radius of gyration is expressed in units of d_p.

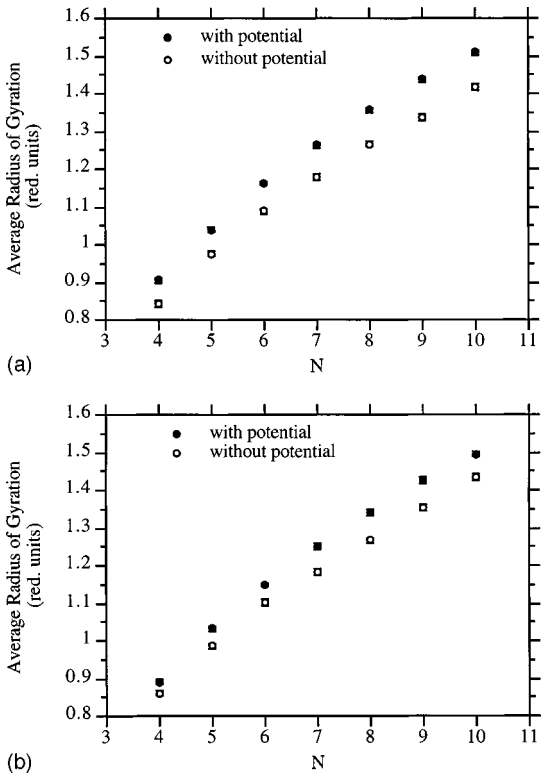

FIG. 10. Interaction potential effect over a range of aggregate sizes for $d_p = 30$ nm at (a) $T = 293$ K and (b) $T = 1500$ K. The radius of gyration is expressed in units of d_p.

tent by the interaction energy.

In the case of free molecular regime particles, Figs. 9(a) and 9(b) together show the effect of temperature on aggregate morphology, with and without potential, over a range of aggregate sizes ($N = 4-10$) using the average radius of gyration to describe the aggregate morphology. The differences in the average r_g with and without the potential almost vanish as the temperature increases from 293 to 1500 K. For transition regime particles, the differences in the average r_g's do not vanish [Figs. 10(a) and 10(b)], though they appear to be somewhat reduced. This can be understood by recalling that the results without potential correspond to the ''infinite'' temperature case, when particle trajectories are linear and the reaction cross section equals the geometric cross section. As the temperature of the simulations with potential increases, the results tend to the ''infinite'' temperature result. The temperature at which the convergence occurs, however, depends on the depth and gradient of the potential well. The potential well for transition regime particles is steeper than for the free molecular regime particles; hence the temperature at which the convergence occurs must be greater than the corresponding temperature for the free molecular case, i.e., greater than 1500 K.

Figures 11(a) and 11(b) show the effect of temperature on average aggregate r_g over the full range of aggregate sizes for the free molecular and transition regimes, respectively. In the free molecular case, the average r_g at 1500 K is consistently lower than that at 293 K, suggesting that the aggregates are more compact. However, for the transition regime, there is no appreciable difference in the radii of gyration at the two different temperatures. The above result is a conse-

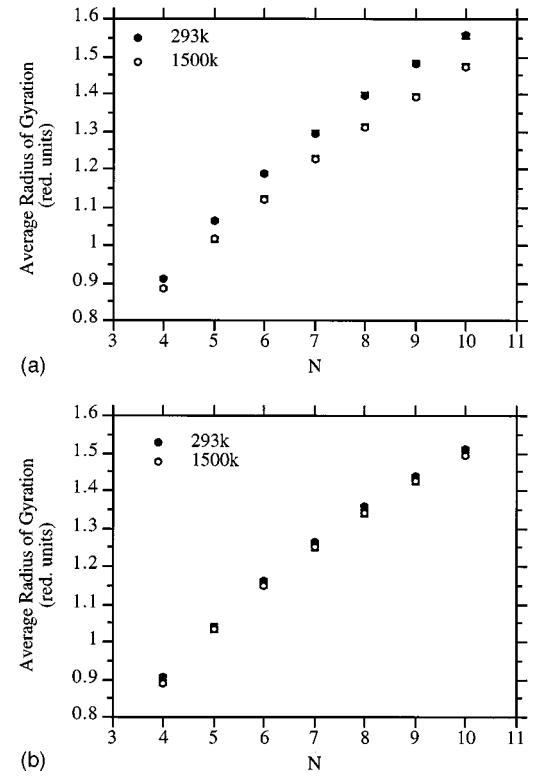

FIG. 11. Average radius of gyration vs aggregate size for $d_p = 6$ nm at $T = 293$ and 1500 K for (a) $d_p = 6$ nm and (b) $d_p = 30$ nm. The radius of gyration is expressed in units of d_p.

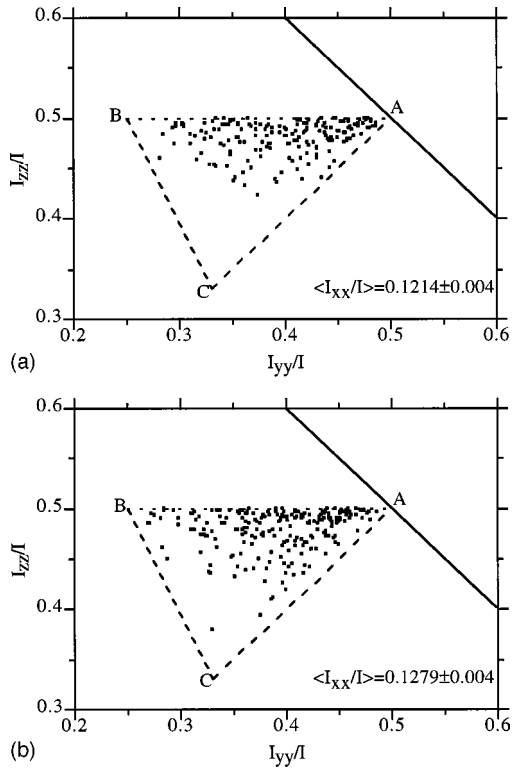

FIG. 12. Scatter plot of I_{yy}/I vs I_{zz}/I for aggregates grown (a) with the potential on, and (b) without the potential at $T=1500$ K. $N=5$ and $d_p=6$ nm.

quence of the very different roles played by the interaction potential in particle transport.

The effect of temperature on the aggregates grown, under free molecular conditions, with and without the potential, can be understood by comparing the differences between the moment of inertia plots, Figs. 4(a) and 4(b) (at 293 K), with the differences between Figs. 12(a) and 12(b) (at 1500 K). At 293 K, the moment of inertia distributions are noticeably different, whereas at 1500 K the difference is barely visible, implying that at high temperatures, the interaction potential effect is overshadowed by the temperature effect.

From Tables III(a) and IV(a) one can see that, for primary particles of diameter 6 nm, as the temperature increases from 293 to 1500 K, and the rate constant enhancement factor Ψ_p decreases from 2.27 ± 0.1 to 1.69 ± 0.1. Ψ_p is a the ratio of $\sigma_p(T)$, the cross section, with potential, at temperature T, to $\sigma_0(\infty)$, the geometric cross section or the cross section at infinite temperature. The decrease in Ψ_p with increasing temperature implies that, as the temperature increases, $\sigma_p(T)\rightarrow\sigma_0(\infty)$. This convergence is due to the fact that as the temperature increases, the kinetic energy of the colliding particles increases and dominates over the interaction potential energy, as a result of which the particle trajectories tend to be more linear like the trajectories at infinite temperature. The hard sphere rate constant enhancement factor Ψ_0 is independent of temperature, as expected. The reason for this result is that Ψ_0 is the ratio of $\sigma_0(\infty)$, the geometric cross section, to $\sigma_{\rm hs}$, the hard sphere cross section, both of which are independent of temperature. Similar conclusions can be made from Tables III(b) and IV(b) for the transition regime particles. However, the ratio $\Psi_p(293)/\Psi_p(1500)$, which is a measure of the change in Ψ_p with temperature, decreases from 1.34, for the free molecular regime particles to 1.17, for the transition regime particles. This is a further indication [40] of the fact that, in the transition regime, the effect of the interaction potential on the particle transport (or collision trajectory) is small.

TABLE IV. Rate constants and rate constant enhancement factors for aggregate-monomer collisions at 1500 K for primary particles of diameter (a) 6 nm and (b) 30 nm. N denotes the number of particles in the aggregate. Subscripts indicate the following: p, with potential; 0, without potential; hs, hard sphere.

N	Rate constants (10^{-9} cm^{-3}/s)			Ψ_p	Ψ_0
	R_p	R_0	$R_{\rm hs}$	R_p/R_0	$R_0/R_{\rm hs}$
			(a) 6 nm		
2	6.19±0.2	3.82±0.2	3.15	1.62±0.1	1.21±0.2
3	7.49±0.2	4.40±0.2	3.47	1.70±0.1	1.27±0.2
4	8.44±0.2	5.00±0.2	3.77	1.69±0.1	1.33±0.2
5	9.51±0.2	5.83±0.2	4.05	1.63±0.1	1.44±0.2
6	10.79±0.2	5.77±0.2	4.32	1.87±0.1	1.34±0.2
7	11.11±0.2	6.42±0.2	4.57	1.73±0.1	1.40±0.2
8	11.75±0.3	7.24±0.2	4.81	1.62±0.1	1.51±0.2
9	12.48±0.3	7.71±0.2	5.04	1.62±0.1	1.53±0.2
				1.69±0.1[a]	1.38±0.2[a]
			(b) 30 nm		
2	13.96±0.5	8.27±0.4	7.04	1.69±0.1	1.17±0.4
3	15.19±0.4	10.09±0.4	7.75	1.51±0.1	1.30±0.4
4	18.23±0.5	11.18±0.4	8.43	1.63±0.1	1.33±0.4
5	20.43±0.5	12.73±0.4	9.06	1.60±0.1	1.41±0.5
6	21.89±0.5	13.57±0.5	9.65	1.61±0.1	1.41±0.5
7	22.82±0.6	15.17±0.5	10.21	1.50±0.1	1.49±0.5
8	25.46±0.6	16.77±0.5	10.75	1.52±0.1	1.56±0.5
9	27.68±0.6	17.80±0.5	11.26	1.56±0.1	1.58±0.5
				1.58±0.1[a]	1.41±0.5[a]

[a]Average rate constant.

D. Pressure effects

In an effort to study the effect of pressure on aggregate structure and collision rates, simulations were performed at two different pressures, 760 and 3040 torr, for a fixed temperature of 293 K and primary particles of diameter 6 nm. An increase in the pressure by a factor of 4, from 760 to 3060 torr, results in a decrease in the mean free path of the gas molecules, λ_g, by the same factor. The Knudsen number, therefore, decreases from 22.49, which is characteristic of the free molecular regime, to 5.62, which is characteristic of the transition regime. The pressure increase manifests itself in the simulations through a reduced jump distance since the jump distance depends on λ_g (see Sec. II B). No significant difference was observed in the structure of the aggregates or in the aggregate-monomer collision rate constants. Intuitively, one would expect that the effect of increased pressure would be more compact aggregates. However, the effect of the interaction potential, being much stronger, masks the pressure effect.

VI. CONCLUSIONS

We have presented a simulation model, based on molecular dynamics methods, for aerosol particle aggregation. We

examined the effects of the retarded long-range van der Waals force, particle transport, and ambient temperature and pressure on aggregate-monomer collision rate constants and aggregate structure. In the free molecular regime (Kn $\geqslant$10), inclusion of the van der Waals force between the aggregating particles results in enhancements in the collision rate constants. Also, the aggregates were tenuous, with few branches, indicating that the incoming monomer tends to stick to the extremities of the aggregate because of the attractive force between the particles. Exclusion of the interparticle forces results in a decrease in the collision rate constants. The aggregates were more compact and branched, indicating that the monomer is more likely to travel to the interior of the aggregate before it collides and sticks to the aggregate. In the transition regime, similar effects were observed, but they were much more subtle, thereby suggesting that the van der Waals force has a much greater influence on particle transport in the free molecular regime than in the transition regime. By comparing the results of the simulations performed with retarded and nonretarded van der Waals forces, we found that the retardation effect causes a decrease in the collision rate constant and a decrease in the openness of the aggregates. These observations suggest that the decrease in the range of the interparticle forces brought about by retardation is responsible for the decrease in the collision cross section, which in turn results in more compact aggregate structures and a decrease in the rate constants. In the free molecular regime, we observed that an increase in the ambient temperature (293–1500 K) resulted in a failure of the tenuous aggregate structures to form in favor of more compact structures (characteristic of the simulations without the forces) and a decrease in the collision rate enhancement factors. However, in the transition regime these effects were less apparent. These results are a consequence of the particle trajectories becoming more linear with increasing temperature, which results in the reaction cross section approaching the geometric cross section. The temperature at which the convergence occurs, however, depends on the depth and gradient of the potential well. The potential well for the transition regime particles is steeper than for the free molecular regime particles; hence the temperature at which the convergence is apparent is higher than for the free molecular case, i.e., 1500 K. No significant difference was observed in the structure of the aggregates or in the aggregate-monomer collision rate constants with increasing pressure. Intuitively, one would expect that the effect of pressure would be more compact aggregates, but this is not the case because the effect of interaction potential is much stronger than the effect of the pressures and therefore overshadows it.

ACKNOWLEDGMENT

This work was supported by the U.S. Department of Energy under Grant No. De-FG05-91-ER61207.

[1] S. R. Forrest and T. A. Witten, J. Phys. A **12**, L109 (1979).
[2] C. M. Megaridis and R. A. Dobbins, Combust. Sci. Technol. **66**, 1 (1989).
[3] R. J. Samson, G. W. Mulholland, and J. W. Gentry, Langmuir **3**, 272 (1987).
[4] W. H. Marlow, Remote Sens. Rev. **8**, 255 (1993).
[5] Y. Crouzet and W. H. Marlow, Aerosol. Sci. Technol. **22**, 43 (1995).
[6] K. Okuyama, Y. Kousaka, and K. Hayashi, J. Colloid Interface Sci. **101**, 98 (1984).
[7] N. A. Fuchs and A. Sutugin, J. Colloid Interface Sci. **20**, 492 (1965).
[8] S. C. Graham and J. B. Homer, Discuss. Faraday Soc. **7**, 85 (1973); W. H. Marlow, J. Colloid Interface Sci. **87**, 207 (1982).
[9] W. H. Marlow, J. Chem. Phys. **73**, 6284 (1980).
[10] V. Arunachalam, W. H. Marlow, and J. X. Lu, Phys. Rev. E **58**, 3451 (1998).
[11] H. J. Herrmann, Phys. Rep. **136**, 153 (1986).
[12] A. Gutsch, S. E. Pratsinis, and F. Loffler, J. Aerosol Sci. **26**, 187 (1995).
[13] M. Eden (unpublished).
[14] M. J. Vold, J. Colloid Interface Sci. **18**, 684 (1963).
[15] D. N. Sutherland, J. Colloid Interface Sci. **22**, 300 (1966).
[16] T. A. Witten and L. M. Sander, Phys. Rev. Lett. **47**, 1400 (1981).
[17] H. B. G. Casimir and D. Polder, Phys. Rev. **73**, 360 (1948).
[18] R. D. Levine and R. B. Bernstein, *Molecular Reaction Dynamics and Chemical Reactivity* (Oxford University Press, New York, 1987).
[19] J. M. Haile, *Molecular Dynamics Simulation: Elementary Methods* (Wiley, New York, 1992).
[20] P. Meakin, Phys. Rev. A **29**, 997 (1984).
[21] M. Kolb, R. Botet, and R. Jullien, Phys. Rev. Lett. **51**, 1123 (1983).
[22] R. D. Mountain, G. W. Mulholland, and H. Baum, J. Colloid Interface Sci. **114**, 67 (1986).
[23] M. W. Williams and E. T. Arakawa, J. Appl. Phys. **43**, 3460 (1972).
[24] E. M. Lifshitz, Zh. Eksp. Teor. Fiz. **29**, 94 (1956) [Sov. Phys. JETP **2**, 73 (1956)].
[25] A. S. Amadon and W. H. Marlow, Phys. Rev. A **43**, 5483 (1991).
[26] J. X. Lu, W. H. Marlow, and V. Arunachalam, J. Colloid Interface Sci. **181**, 429 (1996).
[27] S. K. Friedlander, *Smoke, Dust, and Haze* (Wiley, New York, 1977).
[28] N. A. Fuchs, *The Mechanics of Aerosols* (Pergamon, New York, 1964).
[29] S. N. Rogak, R. C. Flagan, and H. V. Nguyen, Aerosol. Sci. Technol. **18**, 25 (1993).
[30] J. G. Gay and B. Berne, J. Colloid Interface Sci. **109**, 90 (1986).
[31] R. Venkatesh, R. R. Lucchese, W. H. Marlow, and J. Schulte, J. Chem. Phys. **102**, 7683 (1995).
[32] R. N. Porter and L. M. Raff, in *Dynamics of Molecular Collisions*, edited by W. H. Miller, Modern Theoretical Chemistry, Vol. I, Part B (Plenum, New York, 1973), p. 1.
[33] J. Schulte, R. R. Lucchese, and W. H. Marlow, J. Chem. Phys. **99**, 1178 (1993).

[34] J. W. Brady, J. D. Doll, and D. L. Thompson, J. Chem. Phys. **71**, 2467 (1979); **73**, 2767 (1980); **74**, 1026 (1981).
[35] K. L. Lim and R. G. Gilbert, J. Phys. Chem. **94**, 72 (1990).
[36] G. Ciccotti and J. P. Ryckaert, Comput. Phys. Rep. **3**, 345 (1986).
[37] L. Verlet, Phys. Rev. **159**, 98 (1967).
[38] B. B. Mandelbrot, *The Fractal Geometry of Nature* (Freeman, New York, 1982).
[39] W. H. Marlow, Surf. Sci. **106**, 529 (1981).
[40] W. H. Marlow, J. Chem. Phys. **73**, 6288 (1980).